EurJIC
European Journal of Inorganic Chemistry

A Journal of ChemPubSoc Europe

Accepted Article

Title: Cooperative interactions in the second coordination sphere of pyridazine/pyridine containing polyazaheterocyclic iron(II) complexes increase their stability towards protonation.

Authors: Ahmad Hammoud, Jean-Boris Nshimyumuremyi, Jérémie Bourotte, Fabio Lucaccioni, Koen Robeyns, Marinela M Dîrtu, Yann Garcia, and Michael Singleton

To be cited as: *Eur. J. Inorg. Chem.* 10.1002/ejic.201800533

Link to VoR: http://dx.doi.org/10.1002/ejic.201800533

WILEY-VCH

10.1002/ejic.201800533

WILEY-VCH

FULL PAPER

Cooperative interactions in the second coordination sphere of pyridazine/pyridine containing polyazaheterocyclic iron(II) complexes favor protonation.

Ahmad Hammoud, Jean-Boris Nshimyumuremyi, Jérémie Bourotte, Fabio Lucaccioni, Koen Robeyns, Marinela M. Dîrtu, Yann Garcia,* Michael L. Singleton*

Abstract: The new pyridazine containing iron complexes, (N,N,N',N'-tetrakis(3-pyridazylmethyl)propylenediamine)iron(II)$(PF_6)_2$ (**1**) and (N,N'-bis(2-pyridazylmethyl)-N,N'-bis(2-pyridylmethyl)propylenediamine)iron(II) $(PF_6)_2$ (**2**) were synthesized and their reactivity towards protonation was compared to the analogous tetrapyridine complex (N,N,N',N'-tetrakis(2-pyridylmethyl)propylenediamine)iron(II)$(PF_6)_2$ (**3**). The solution and solid state structures were confirmed by NMR and X-ray crystallographic studies. For **1**-**3**, the ligands bind in a hexadentate fashion giving similar octahedral structures with an N_6 coordination environment. Across the series, the increasing number of pyridazines has only modest effects on the spectroscopic and electrochemical properties of the metal. Nevertheless, their reactivity towards protonation is drastically different. While **2** and **3** decompose in the presence of strong acids, **1** is able to be stably protonated as a result of cooperative second sphere interactions.

Introduction

First row transition metal complexes containing pyridazine like moieties have attracted interest for applications in medicine, materials development, and catalysis.[1-10] In these systems, the pyridazine ring provides a number of important effects for tuning the properties and reactivity of the metal complex. Notably, the presence of the second nitrogen gives additional reactive sites in the second coordination sphere for interaction with other molecules or substrates.

Relative to the analogous pyridine ligands, pyridazines have distinctly different electronic properties that can alter the properties of the metal site. The second nitrogen decreases its σ-donating ability and also makes it a better π-acceptor.[11] Additionally, for coordination, pyridazine can act as a bridging ligand, potentially leading to the formation of more complex multimetallic structures.[12-20] However, for first row transition metals, this generally requires that the pyridazine is part of a larger ligand scaffold or macrocycle functionalized with additional pendant donor sites. In the absence of this cooperation and notably in higher valent metals, pyridazines typically coordinate in a monodentate fashion through a single nitrogen.[21-30] This is likely due to the initial coordination with the first nitrogen decreasing the basicity of remaining site for interaction with an additional metal. Despite this potential for deactivation, examples of metal bound pyridazines have been reported where the basicity of the additional endocyclic nitrogen is potentially important for reactivity.

As an example, Yang and co-workers[10] recently described a number of iron based catalysts for water oxidation where pyridine groups where substituted for pyridazines in tetradentate ligands. They proposed that the additional nitrogen could act as a proton relay during the deprotonation steps in the catalytic cycle and showed that it could retain some basicity. Nevertheless, the new complexes showed similar reactivity for water oxidation as compared to the analogous pyridine complexes. Interestingly, for unbound pyridazines, their role in proton transfer during catalysis has been shown to be more significant despite the basicities of these systems being reported as similar.[5-6] As few examples of iron bound pyridazines have been reported, the synthesis of this type of complex and the study of their reactivity could lead to a better understanding of the factors that might alter their ability to participate in proton transfer steps and extend their potential for catalytic applications.

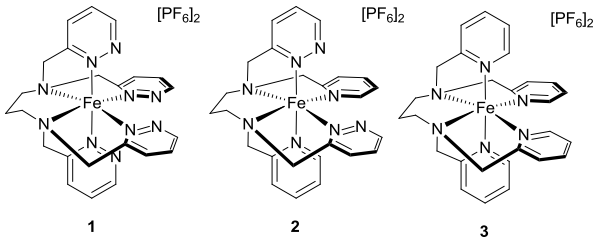

Figure 1. Series of polypyridyl/pyridazyl Fe(II) complexes studied.

To this end, we designed a series of pyridazine containing iron complexes using analogs of the ligand N,N,N',N'-tetrakis(2-pyridylmethyl)-1,3-propylenediamine (tptn),[31-34] Figure 1, where four (**1**) or two (**2**), of the pyridine groups have been replaced by pyridazine and compared these to the complex of the unmodified tetrapyridine ligand (**3**). Relative to iron complexes of the related N,N,N',N'-tetrakis(2-pyridylmethyl)-1,2-ethylenediamine (tpen) ligand, which have been widely studied for both their interesting spin-crossover behavior and as mimics of superoxide dismutase,[31-32,35-46] the Fe(tptn) complexes have received significantly less attention. This is in part due to their high stability,

A. Hammoud, J.-B. Nshimyumuremyi, J. Bourotte, F. Lucaccioni, K. Robeyns, M. M. Dîrtu, Y. Garcia, M. L. Singleton
Institute of Condensed Mater and Nanosciences, Molecules, Solids and Reactivity (IMCN/MOST)
Université catholique de Louvain
Place L. Pasteur 1, 1348 Louvain-la-Neuve, Belgium
E-mail: m.singleton@uclouvain.be, yann.garcia@uclouvain.be
https://uclouvain.be/en/research-institutes/imcn/most/michael-singleton.html; http://ygarcia.homestead.com/index.html

Supporting information for this article is given via a link at the end of the document.

both towards oxidation as well as to ligand substitution by solvent, and their stable low-spin ground state.[31,47] While this stability limits the applications of the Fe(tptn) complexes, it does provide an ideal scaffold for studying the effects of the pyridine/pyridazine substitutions and the reactivity of the second sphere nitrogens. Herein we describe the full characterization of **1**, **2**, and **3** by NMR, UV-Vis, and Mössbauer spectroscopies, as well as, by cyclic voltammetry and X-ray crystallography. Despite having similar structural and electronic properties, studies on the protonation behavior of the complexes show that cooperativity between multiple nitrogens in the second coordination sphere lead to a dramatic change in the acidic stability and reactivity of **1** versus either **2** or **3**.

Results and Discussion

Synthesis of ligands and complexes

The pyridazine containing polyazaheterocyclic ligands were synthesized in a manner similar to reported procedures for the tetrapyridine ligand, N,N,N',N'-tetrakis(2-pyridylmethyl)propylenediamine (**L3**).[47-48] Alkylation of 1,3-propylenediamine or N,N'-bis(2-pyridylmethyl)propylene diamine with 3-(chloromethyl)pyridazine, Scheme 1, affords ligands **L1** & **L2** in moderate yield, 50-70 %.

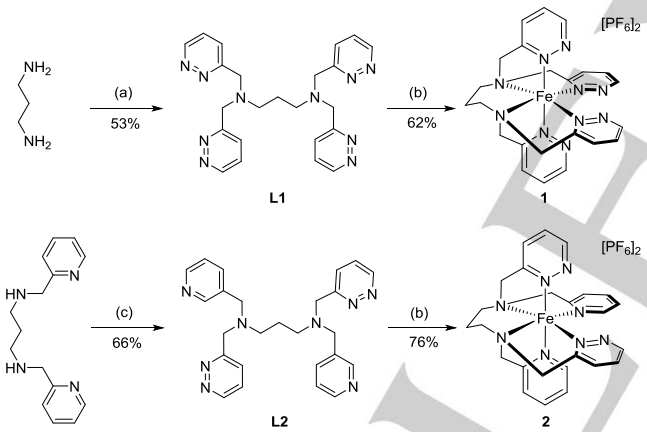

Scheme 1. Synthesis of complexes 1 and 2: (a) 3-(chloromethyl)pyridazine, KBr, K_2CO_3, MeCN, Δ; (b) $FeCl_2$, KPF_6, H_2O; (c) 3-(chloromethyl)pyridazine hydrogen chloride, K_2CO_3, MeCN

For these reactions, the synthesis of the 3-(chloromethyl)pyridazine was initially accomplished through the chlorination of 3-methylpyridazine using trichloroisocyanuric acid.[49] However, other methods offered better results. Notably, the chlorination of pyridazin-3-ylmethanol,[50] which is easily synthesized from furfuryl alcohol (see SI) using a minor variation of established procedures,[51-52] provides a more scalable and consistent route to the stable 3-(chloromethyl)pyridazine hydrochloride salt. Using the material obtained following this approach, the incorporation of the pyridazyl unit into **L1** and **L2** can occur more cleanly which allows for easier isolation of the ligands.

The complexes **1**, **2**, and **3** were synthesized by addition of one equivalent of $FeCl_2$ to an aqueous solution of the respective ligand. An immediate color change from light yellow to dark red is observed upon metal addition. The complexes can then be precipitated from solution as red-orange powders by addition of KPF_6. All three are air-stable over the course of several days both as solids and in solution. They are highly soluble in MeCN, but only moderately soluble in alcohols or water at room temperature.

^{1}H NMR spectra of **1**, **2**, and **3**, Figure 2, show relatively sharp signals over a limited spectral range. This is consistent with the diamagnetic nature of low spin iron(II) in an octahedral geometry, a geometry that would be expected if the ligand binds in a hexadentate fashion, and matches well with the magnetic behavior previously reported for the perchlorate salt of **3**.[32]

For all three complexes, octahedral coordination should result in axial chirality. In the NMR, this should lead to the splitting of the resonances for both the benzylic methylene and the -CH_2 units of the propylene linker into diastereotopic pairs. For **1** and **3**, this is observed by the presence of four doublets, integrating for two each, between 4.0-5.0 ppm for the benzylic -CH_2 units. The number of signals fits with the fact that the homogenous ligand sets (all pyridazine or all pyridine) for these complexes should result in a 2-fold symmetry axis that makes both of the equatorial aromatic rings equivalent and both of the axial rings equivalent. The presence of this symmetry element also supports the hexadentate binding by the ligand and the octahedral geometry of complexes **1** and **3**.

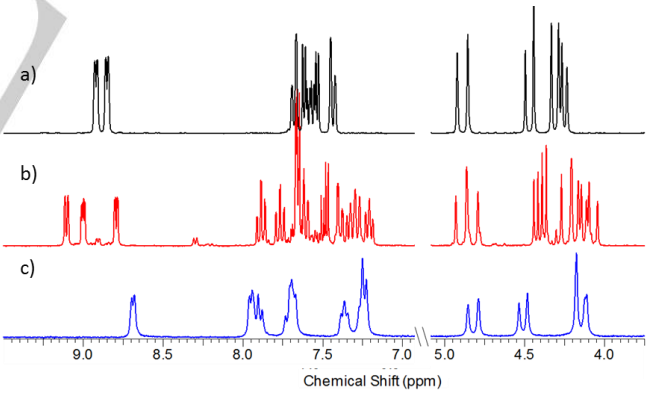

Figure 2. Comparison of the ^{1}H NMR spectra in CD_3CN of complexes **1** (a), **2** (b), and **3** (c) in the regions between 3.5-5 ppm and 7-9.25 ppm.

The situation is more complicated for **2**. Each aliphatic nitrogen has one pyridine and one pyridazine, making multiple conformations possible. Using the positions of the pyridazines to describe these and assuming octahedral geometry, the complex could adopt a conformation where both pyridazines are axial, both equatorial, or one axial-one equatorial. The two former conformations should both exhibit C_2 symmetry similar to complexes **1** and **3**, while the latter would lack this symmetry and

a greater number of signals would be expected. The presence of eight doublets for the benzylic protons and the doubling of the number of aromatic signals supports the axial-equatorial conformation as the major species for this complex. A second species (10% by integration) can also be observed in the spectra for **2**. This has been assigned as one of the higher symmetry conformers due to the presence of only two aromatic signals at 8.3 and 8.9 ppm for the C-H groups adjacent to the endocyclic nitrogens and four doublets between 4.0 - 5.0 ppm for the benzylic CH_2 groups. Nevertheless, despite our best efforts, this minor compound could not be separated from the major species and so this assignment remains tentative.

Interestingly, despite being similar in the unbound ligands, for **1**, **2**, and **3** the chemical shift for the resonances for the 6-position protons (C-H adjacent to the endocyclic nitrogens in the pyridazine or pyridine units) vary significantly from complex to complex. In **1**, the two signals for this position in the pyridazines are observed just below 9.0 ppm with only 0.06 ppm difference in the shifts. In the corresponding tetrapyridine complex, one of the signals is observed at 8.7 ppm, while the second appears significantly upfield shifted at 7.9 ppm. A similar upfield shift is observed for one of the pyridine 6-position resonances in **2**, (it appears at ~7.7 ppm) while the resonances for the 6-position in the remaining three heterocycles appear between 8.8 and 9.2 ppm. We postulate that the observed shift is due to the positioning of the axial pyridine 6-position C-H directly above one of the equatorial rings, thus leading to shielding of this proton due to the aromatic ring current effect. In the case of the axial pyridazines, this C-H would be positioned further away from the equatorial rings (equivalent to the 5-position on the pyridine rings) and be affected less by the π-system of the equatorial aromatic group. Thus for complex **2**, the large observed shift for only one of the pyridine 6-position protons could additionally be expected for the axial/equatorial conformation described above.

Solid state structures

Further support for the structures of each complex were obtained from X-ray diffraction studies. Single crystals of X-ray quality for **1** and **2** were obtained by a three layer approach. Hexane was first layered onto solutions of the complexes in MeCN, followed by addition of toluene on top of the hexane. After diffusion of the toluene into the MeCN crystals were obtained. For complex **3**, crystals were grown by slow diffusion of an MeCN solution of **3** into $CHCl_3$. Complexes **1** and **2**, crystalize in the monoclinic space groups $P2_1/c$ and $P2_1/n$ respectively. **1** crystalizes with two molecules of MeCN per complex (Z=4) in the unit cell and **2** crystallizes as the monosolvated MeCN species. While the perchlorate salt of **3** has been reported,[32] attempts at obtaining an X-ray structure of this complex have been previously unsuccessful and only limited crystallographic details have been reported. In the case of the PF_6^- salt reported herein, structural refinement was also complicated due to the instability of the crystals outside the crystallization solution. The final structure shows very large cavities ca. 40% of the total cell volume, present as open column running along the c-axis. It is believed that the volatile MeCN emerges almost instantly from the crystal when removed from the mother liquid, this is further evidenced by the appearance of fissures on the crystal surface within moments after crystal manipulation. Transfer to a viscous oil slowed down this process and enabled mounting and flash cooling of the crystal. Given the limited crystal quality, a resolution cut-off of 1Å was imposed during integration and refinement. The structure was determined by Molecular Replacement[53] in $P6_5$, as direct methods failed due to the initially undetected twinning around the reciprocal b axis, combined with twinning by inversion. Possibly the reported ClO_4^- analogue of **3** suffered from the same issues and although no cell parameters were given, with the postulated unit cell volume of ca. 7000 $Å^3$ and the hexagonal system a similar desolvated structure might be hypothesized, likewise the theorized space group $P6_522/P6_122$ might be the higher metric symmetry often encountered with twinning.[32]

Refinement converged without distance and angle restraints for the Fe complex **3**, similar restraints were used for the disordered PF_6^- anions. Both were found to be disordered, one showed two-fold disorder in an almost 50/50 ratio. The other was refined over 3 parts with a 50/30/20 ratio. Refined twin fractions (4 domains) indicate a 48% contribution of the main domain with a 40% contribution of the inverted rotation around the reciprocal b axis. The remaining two domains have a combined contribution of about 10%. Diffuse solvent contribution to the diffraction intensities was treated by the squeeze procedure in Platon.[54] Crystallographic and refinement details are tabulated in the supporting information.

The crystal structures of **1**, **2**, and **3**, Figure 3, each show a single iron center bound in a hexadentate fashion by their respective ligands. The metal centers exhibit a distorted octahedral geometry with a N_6 coordination environment consisting of the two aliphatic amines of the propylene diamine linker and four endocyclic nitrogens provided by the pendant pyridine or pyridazine units. Relevant structural metrics are given in Table 1. To compare the overall geometry of the three complexes the RMS deviations between each pair were calculated, revealing that all three complexes are highly similar with calculated values of 0.12 $Å^2$ between 1 and 2 and 0.21 Å2 between **1** and **3** (and between **2** and **3**).

The reported Fe complexes show pseudo C2-symmetry, with the 2-fold axis passing though the equatorial plane (See Figure 3). In **2**, the mixed pyridine/pyridazine complex, the 2-fold symmetry is broken by a cis-equatorial configuration of the pyridine and pyridazine moieties, but otherwise maintains the global appearance throughout the three complexes. The $Fe\text{-}N_{propylene}$ distances in the complexes range between 1.89-2.04 Å, which is on the short end of the distance range found in the CSD for Fe – tertiary amine distances (< 2.215 Å >). Direct comparison between the Fe-pyridine or Fe-pyridazine bond distances based on complexes **1** and **3** is complicated due to the disparity in values observed for the four pyridine groups in **3**. Indeed, while the $Fe\text{-}N_{heterocycle}$ distances in **1** only range between 1.945-1.959 Å, in **3** the Fe-pyridine distances display a much larger variation, 1.907-2.005 Å. However, in the mixed pyridine/pyridazine containing **2**, the $Fe\text{-}N_{pyridazine}$ bonds appear to be moderately shorter (1.951 and 1.944 Å) than the $Fe\text{-}N_{pyridine}$ distances (1.961 and 1.985 Å). Nevertheless, for all of the rings, these values remain well within the range of the analogous tpen or polypyridyl Fe complexes and

are similar to values reported for Fe-N distances in other low-spin Fe(II) complexes.[31-47]

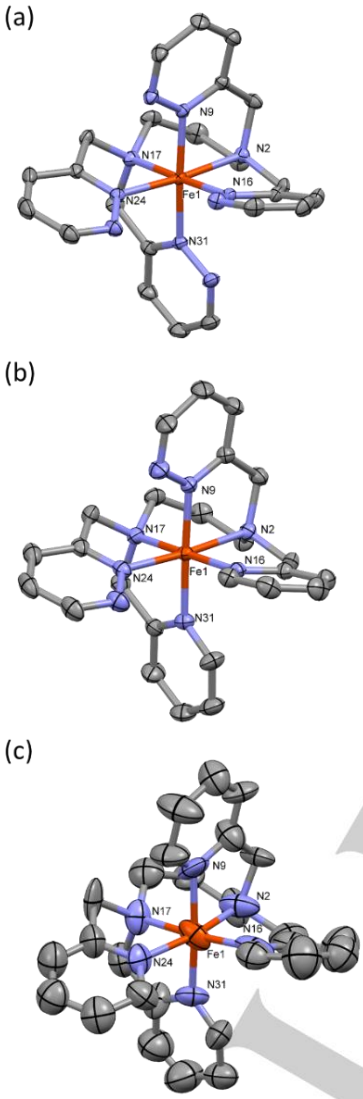

Figure 3. Thermal ellipsoid plots (50%) of **1** (a), **2** (b), and **3** (c). Numbering for the three complexes corresponds to the numbering in Table 1. Hydrogen atoms and PF_6^- counter ions have been omitted for clarity.

In fact, the only major differences from the tpen derivatives are observed in the angles around the iron center. The propylene linker used in **1**-**3** results in a greater bite angle for the aliphatic nitrogens to iron (~90 – 95 °) as compared to derivatives with the ethylene linker (<86 °). This relaxed angle also leads to a ~10 ° decrease in the bite angle for the equatorial heterocyclic ligands to iron. As a result, the distance between these aromatic units also decreases, placing the *ortho* N or C of the equatorial rings at 2.935, 3.066 and 3.233 Å from each other for **1**, **2**, and **3** respectively. In **1**, this separation between the unbound nitrogens

Table 1. Comparison of selected structural metrics for complexes **1**, **2**, and **3**.

Distance (Å)	1	2	3
Fe-N2	2.038(1)	2.044(2)	1.890(15)
Fe-N31	1.945(1)	1.961(2)	1.907(13)
Fe-N24	1.946(1)	1.951(2)	1.926(15)
Fe-N9	1.959(1)	1.944(2)	1.984(8)
Fe-N17	2.013(2)	2.030(2)	1.991(13)
Fe-N16	1.948(1)	1.985(2)	2.005(19)
Angle (°)			
N31-Fe-N24	90.70(6)	88.92(6)	87.5(6)
N31-Fe-N16	96.18(6)	94.55(6)	99.6(6)
N31-Fe-N2	92.12(6)	93.25(6)	92.8(6)
N31-Fe-N17	84.18(6)	84.41(6)	82.9(6)
N31-Fe-N9	175.68(6)	177.18(6)	174.3(5)
N24-Fe-N9	93.35(6)	93.85(6)	93.7(5)
N24-Fe-N16	100.70(6)	101.67(7)	105.0(7)
N24-Fe-N17	81.22(6)	81.29(7)	79.4(6)
N16-Fe-N9	84.55(6)	85.42(6)	85.4(5)
N16-Fe-N2	82.98(6)	83.10(6)	85.5(8)
N9-Fe-N17	94.96(6)	95.47(6)	91.9(5)
N9-Fe-N2	83.74(6)	83.94(6)	85.1(5)
N17-Fe-N2	95.08(6)	93.98(6)	90.1(7)
Dihedral Angle (°)[a]			
Equatorial Aromatic Rings	34.2	28.3	41.8
Axial Aromatic Rings	79.0	89.8	81.6

[a] Defined as the angle between the planes of the equatorial or axial aromatic rings

in the pyridazine rings could potentially allow them to act in a bidentate or cooperative fashion. However, the dihedral angle for these rings is significantly deviated from the coplanar conformation ideal for this purpose. We observe across the series of complexes that this angle (measured as the angle between the planes of equatorial aromatic rings) increases from 28.3 ° in **2** to 34.2 ° in **1** and ~41 ° in **3**. The larger angle in **3** likely results from the minimization of the steric interaction between the 6-position C-H groups, but may additionally be influenced by a possible C-H--F interaction between the PF_6^- counter ion and the 6-position C-H of one of the equatorial pyridines based on the observed short F-C distance of 1.997 Å.

UV-vis spectra and Mössbauer Analysis

The UV-vis spectra for complexes **1**-**3**, recorded in MeCN, are shown in Figure 4. Wavelength and molar absorptivity data are given in Table 2. The spectra of **3** is in good agreement with the previously reported UV-vis studies of its perchlorate salt.[33] Below 300 nm the spectra of all three complexes are similar, showing two absorptions, one between 205-209 nm and another between 242-252 nm. Based on the low wavelengths and high molar absorptivity values, these are assigned to π-π^* transitions in the ligands.[55] While these remain largely similar across the series, the nature of the heterocycles on the ligand has a stronger influence on the absorptions at higher wavelengths.

Despite being weaker σ-donors than pyridine, pyridazines are typically better π-acceptors. As a result, their incorporation into the ligands has a significant impact on the observed MLCT bands. The tetrapyridine complex, **3**, shows an absorption maxima at 421 nm which has been previously assigned as an MLCT band.[33] This absorption is bathochromically shifted in the tetrapyridazine containing **1**, appearing at 449 nm, and has a molar absorptivity significantly higher than that observed for **3**. Given the analogous nature of complexes **1** and **3**, this absorption has also been assigned as an MLCT band. For **2**, two different absorption maxima are observed, one at 384 nm and the other at 458 nm, with similar molar absorptivities as **3**. These bands overlap well with the MLCT absorptions from **1** and **3**, and are assigned as, for 384 nm, the MLCT from iron to pyridine and, for 458 nm, from iron to pyridazine. No other absorptions were observed above 600 nm.

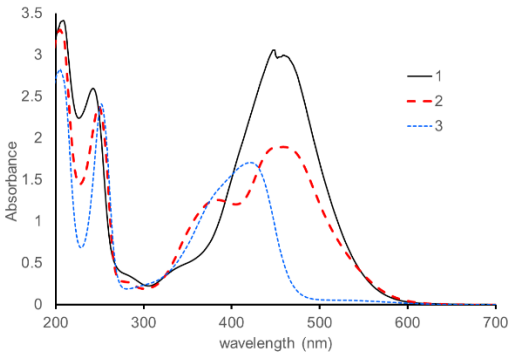

Figure 4. Comparison of the UV-vis spectra in CD_3CN of complexes 1 (a), 2 (b), and 3 (c). Concentration = 0.2 mM.

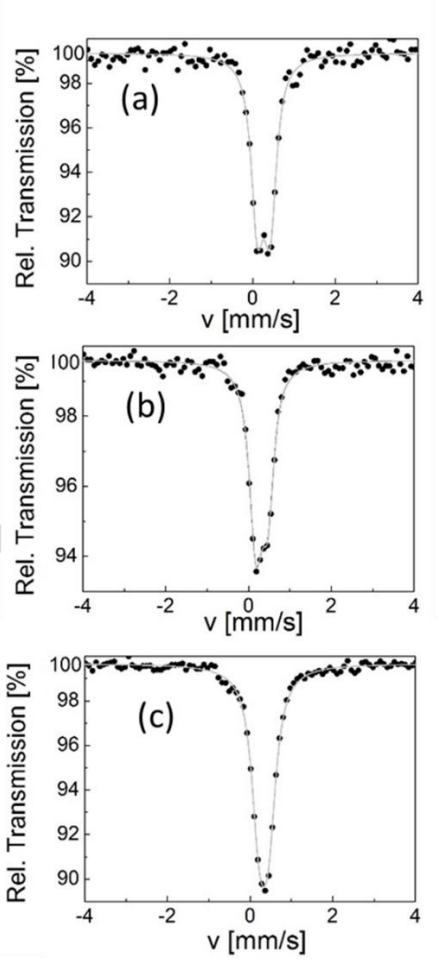

Figure 5. ^{57}Fe Mössbauer spectra for **1** (a), **2** (b), and **3** (c) recorded at 77 K.

Mössbauer spectra of complexes **1**-**3**, Figure 5, with natural abundance ^{57}Fe were collected at 77 K. The Mössbauer parameters are given in Table 2. All three complexes can be fitted to a single quadrupole doublet with parameters consistent with low-spin iron(II), as expected by the solution NMR studies and the magnitude of molar absorption observed in the UV. The isomer shift, δ, is slightly lower for **1** with δ = 0.27 mm/s compared to the one of **2** and **3**, while the quadrupole splitting, ΔE_Q, is identical for **1** and **2**, compared to **3**. This lower quadrupole splitting for **3** points to a lower distortion degree of the iron(II) coordination sphere because of the absence of any electric field gradient contribution to ΔE_Q in the low-spin state.

Table 2. ^{57}Fe Mössbauer parameters for complexes **1**-**3**

Complex	**1**	**2**	**3**
T [K]	77	77	77
δ [mm/s]	0.27(2)	0.33(1)	0.33(1)
ΔE_Q [mm/s]	0.30(2)	0.29(1)	0.22(2)
$\Gamma/2$ [mm/s]	0.16(1)	0.15(1)	0.20(1)
Relative Area [%]	100	100	100
Sites	LS	LS	LS

δ: isomer shift (with respect to α-Fe at r.t.); ΔE_Q: quadrupole splitting; $\Gamma/2$: half width at half maximum; LS: low spin

Cyclic Voltammetry

The presence of the pyridazine units also has a moderate effect on the electrochemical properties of the complexes. The potentials for the oxidations and reductions (vs FcH/FcH+) are shown in Table 3. The voltammograms of **1**-**3**, Figure S1, each show a reversible oxidation event, Figure 6, and one or more irreversible reductions. For **1**, the reductions are observed at -2.25 V and -1.94 V, while complexes **2** and **3** each only show a single event, at -1.99 V and -2.23 V respectively within the electrochemical window.[33]

A single reversible oxidation event is also observed for **1-3** and is assigned to the $Fe^{II/III}$ couple.[33] Relative to complex **3**, which has an oxidation at 0.44 V, the oxidation in **1** and **2** occur at more positive potentials (0.56 V and 0.52 V respectively). Given the similar structures of **1**-**3**, the positive shift observed for both the oxidation and reduction potentials in **1** and **2** should thus only be due to the increased number of pyridazines. This shift does not appear to be linearly correlated with the number of pyridazines as the exchange of two pyridines for pyridazines in **2** results in a change of ~80 mV but the additional substitution of two pyridines (**2** to **1**) only gives a 40 mV increase in the oxidation potential. Still, the overall change is consistent with the metal being less electron rich as the number of pyridazines increases.

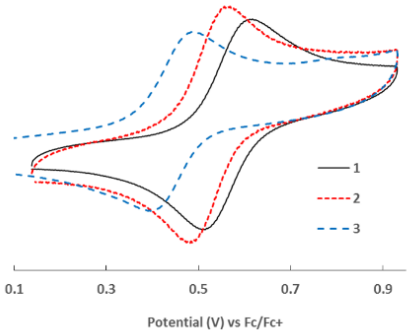

Figure 6. Cyclic voltammograms showing the reversible oxidation for complexes **1**, **2**, and **3**. [**1**] = [**2**] = [**3**] =0.001 M in MeCN with 100 mM $TBABF_4$. All values are reported versus FcH/FcH^+.

Table 3. Electrochemical data for complexes **1**, **2**, and **3**.

	Potential vs FcH/FcH^+ (V)		
Complex	E_{red}	E_{red2}	$E_{ox\ 1/2}$
1	-1.94	-2.25	0.56
2	-1.99		0.52
3	-2.23		0.44

Solvent = MeCN; [Fe] = 1mM; [$TBABF_4$] = 100mM; Scan rate = 100 mV/s

Protonation Behavior

To study the protonation behavior of Fe(II) bound pyridazines, we initially performed a UV-vis titration of **1**-**3** with trifluoroacetic acid. We were surprised to observe that the second sphere nitrogens in these complexes are relatively inert. In fact, **1** shows little to no change by Uv-Vis even upon addition of 100 equivalents of trifluoroacetic acid. Relative to the literature examples where bound counter-ions likely limit the electrostatic destabilization of the protonated species,[10] it is proposed that in **1**, the positive charge of the complex additionally disfavors the protonation with trifluoroacetic acid. This effect should be able to be countered by using a stronger acid. Indeed, **1** could be protonated when triflic acid was used for the titrations.

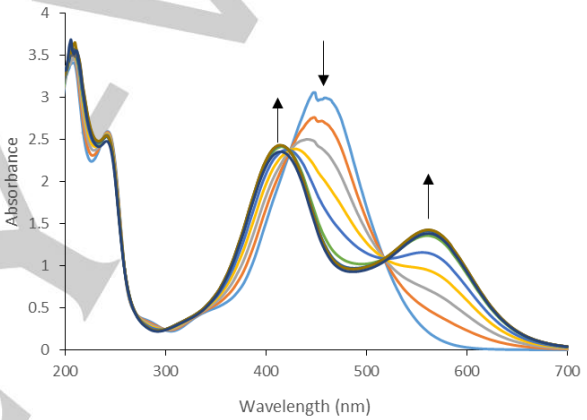

Figure 7. Uv-vis spectra of the titration of 1 (0.2 mM) with 0 - 2 equivalents of TfOH in acetonitrile.

Addition of one equivalent of triflic acid to **1** in MeCN leads to a noticeable color change from red to dark purple. In the UV-vis spectra, Figure 7, the intensity of the MLCT band at 449 nm decreases with added triflic acid, while two new bands appear at 415 and 564 nm. This large change for the MLCT bands could be expected if protonation occurs at the pyridazine nitrogens. Isosbestic points, observed at 421 and 515 nm, are consistent with conversion of **1** into a single new species. This new species appears to be moderately stable to additional acid and a significant decrease in the intensity of the new bands corresponding to ligand dissociation is only observed after addition of multiple equivalents of the acid. By ^1H NMR, Figure 8, as the amount of acid is increased, the signals corresponding to the initial product begin to broaden and shift but remain a single set of signals. This would fit with protonation where the proton transfer equilibrium between the complexes is fast on the NMR timescale. With additional acid, the broad resonances quickly sharpen and a new set of signals appear. Based on the number of signals and the narrow peak widths observed, the new species

is structurally similar to **1** and retains the diamagnetic character of the parent complex. Notably, the presence of four doublets corresponding to the benzylic -CH_2 groups is good evidence that the C_2 symmetry of **1** is still present in the new species and that dissociation of one of the pyridazine rings has not occurred. The largest shifts observed occur in the aromatic region where it appears that the resonances corresponding to one pair of the pyridazines shifts downfield by more than 0.5 ppm, while only minor shifts occur for the resonances corresponding to the other pair. Importantly, these spectral changes are fully reversible. The new species can be converted back into **1** by addition of triethylamine, (See SI, Figure S2), further supporting the fact that the changes to the complex are due to protonation. Based on the above observations, it is proposed that this protonation occurs at an equatorial pyridazine and is likely stabilized through interaction with the second nitrogen of the neighboring equatorial pyridazine, Scheme 2A. Further support for protonation in this position and the need for the additional interaction to stabilize the protonated species comes from comparison to the reactivity of the two other complexes.

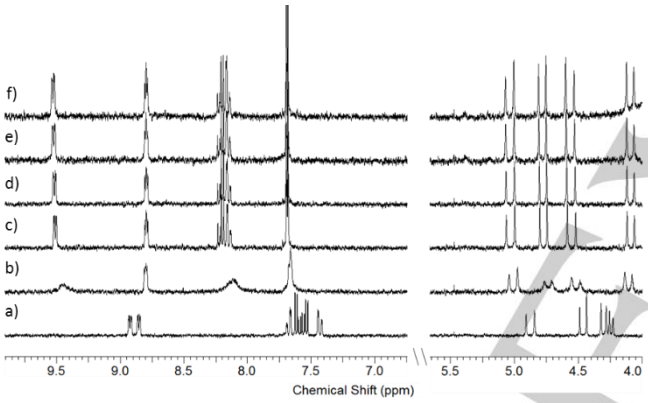

Figure 8. ^{1}H NMR spectra of the titration of (a) **1** (2 mM) with (b) 0.2; (c) 0.4; (d) 0.6; (e) 0.8 and (f) 1.0 equivalents of TfOH in CD_3CN.

In contrast to **1**, neither complex **2** nor **3** show evidence of a stable protonated species. Rather, even with less than one equivalent of acid, ligand dissociation occurs as evidenced by both UV-vis and ^{1}H NMR studies, Figures S3-S6. Upon addition of triflic acid to complexes **2** and **3**, a gradual loss of color is observed. In the UV-vis spectra, Figures S2 and S3, this coincides with a decrease and eventual disappearance of the MLCT bands, while the higher energy bands assigned to the π-π* transitions of the ligand show only minor differences. In the ^{1}H NMR spectra of both complexes, Figures S4 and S5, the addition of one equivalent of acid leads to complete loss of the diastereotopicity observed for the benzylic signals. For **3**, these become a single signal at 4.25 ppm, while for **2**, two different resonances for the benzylic positions are observed at 4.6 and 4.7 ppm consistent with the presence of the two types of pendent heterocycles in the ligand. These changes would be expected upon dissociation of the ligand. It is also important to note that for these complexes no broad signals indicating fast exchange are observed and that the second set of signals corresponding to the dissociated ligands begin to appear even with sub-stoichiometric amounts of the acid.

While this reactivity is unsurprising for **3** as no additional basic sites are present in the ligand, if protonation in **1** was solely due to the presence of the additional nitrogens, the pyridazine rings in **2** should have allowed protonation of the complex prior to degradation. We postulate that the dissimilarity in reactivity of **1** compared to **2** is due to the difference in the second coordination sphere resulting from the axial-equatorial conformation of the pyridazine rings in **2**. Looking at the potential protonation sites in these molecules, Scheme 2, there are two possibilities for the protonation of the pyridazines. Either an equatorial pyridazine or an axial pyridazine can be protonated. Based on the presence of the C-H groups in similar positions in **3**, protonation of the pyridazine group in either position should not be prohibited due to steric factors. If the protonation were to occur in the axial position, both complexes **1** and **2** should show similar reactivity towards protonation since the resulting structural motif would be identical i.e. a protonated pyridazine oriented above an equatorial pyridazine ring, Scheme 2C&D. By contrast, equatorial pyridazine protonation would lead to the proton being in two different local environments in **1** versus **2**, Scheme 2A&B. In **1** the proton would be oriented towards the nearby nitrogen of the neighboring pyridazine. The distance between the two second sphere endocyclic nitrogens (2.9 Å) and the identical pKa of these sites should allow for moderate strength hydrogen bond formation. As such the two nitrogens can act in a cooperative fashion to stabilize the proton. In **2**, no such interaction is possible. Protonation of the equatorial pyridazine would orient the proton towards the 6-position C-H of the neighboring equatorial pyridine which would not provide any stabilizing interaction. The lack of any such interaction combined with the weak basicity of the pyridazine nitrogens is likely what prevents **2** from being stably protonated. These results highlight the potential of multiple cooperative interactions in the second coordination sphere of metal complexes for controlling and modifying reactivity.

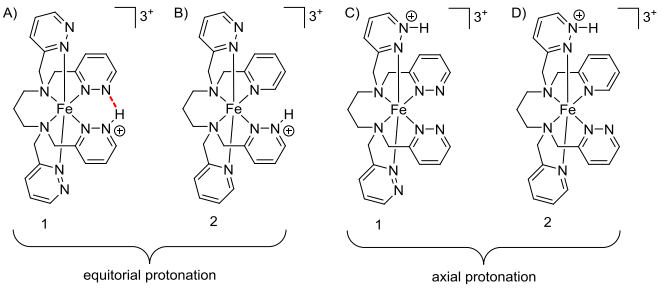

Scheme 2. Comparison between potential protonation sites in **1** versus **2** with potential cooperative interactions (shown in red) that may stabilize protonation.

Conclusions

A series of polyazaheterocycle containing mononuclear iron complexes, including two novel pyridazine containing complexes,

were synthesized and characterized by NMR, UV-vis and Mossbauer spectroscopies, as well as by X-ray diffraction and electrochemical studies. Both solution and solid state studies indicate that all three compounds have similar octahedral structures. Across the series, the increasing number of pyridazines has only modest effects on the spectroscopic and electrochemical properties of the metal. Nevertheless, despite the similarities across the complexes, their reactivity towards protonation is drastically different. While addition of a strong acid to both the tetrapyridine containing **3** and the bispyridazine/bispyridine containing **2** leads only to degradation of the complex due to ligand dissociation, the tetrapyridazine containing **1** is able to be stably protonated. Based on the spectroscopic studies, the protonation of **1** occurs in the equatorial position and is likely stabilized by cooperative interactions between the second coordination sphere nitrogens.

Given the interest that pyridazines have attracted as pendant bases or proton relays in catalysis[5,6,10] the above observations may offer some insight into the design of new systems. While the pyridazines can, in some cases, retain moderate basicity even upon binding to a metal center, our results demonstrate that this is certainly not always the case. The basicity of these systems, as well as their stability in acidic media, has a strong dependence on the specific structure and charge of the corresponding complex. This has the consequence of potentially limiting the range of applicability of metal bound pyridazines, or similar groups with exogenous basic sites, for catalytic purposes. Nevertheless, the current study also shows that by taking into account other groups in the second coordination sphere and designing new systems with additional cooperative interactions, both the stability of the metal complex and the basicity of the groups may still be able to be fine-tuned to allow the additional nitrogens to have some reactivity. For complexes where protonation is more favored, this could significantly augment the ability of these groups to participate in proton transfer steps during catalysis.

Experimental Section

General Procedures. Unless otherwise stated all solvents and reagents were used without further purification. When required, dry solvents were obtained directly prior to use by distillation from CaH_2 ($CHCl_3$, toluene, DCM) or from sodium/benzophenone (THF, Et_2O). Anhydrous acetonitrile was purchased from Sigma or Alfa Aesar. N,N'-bis(2-pyridylmethyl)propylenediamine[56] and N,N,N',N'-tetrakis(2-pyridylmethyl)propylenediamine[48] (**L3**) were synthesized according to reported procedures. NMR spectra were recorded on a Bruker 300MHz Ultrashield™. ^{1}H and ^{13}C NMR chemical shifts are reported in ppm and are calibrated against residual ^{1}H and ^{13}C solvent signals of $CDCl_3$, CD_3CN, or DMSO. Coupling constants are reported in hertz. The following notation is used for the ^{1}H NMR spectral splitting patterns: singlet (s), broad singlet (bs), doublet (d), triplet (t), multiplet (m). UV-visible experiments were performed on a VWR UV-1600PC Scanning Spectrophotometer equipped with Deuterium/Tungsten Halogen Lamp. HR Mass Spectra were recorded by the Mass Spectrometry service of the ASM platform of the Institute of Condensed Matter and Nanosciences at the Université catholique de Louvain. Mössbauer spectra were recorded in transmission geometry with a conventional Mössbauer spectrometer equipped with a ^{57}Co(Rh) radioactive source operating at room temperature. The samples were sealed in aluminum foil and mounted on a nitrogen Oxford bath cryostat. The spectra were fitted to the sum of Lorentzians by a least-squares refinement using or Recoil 1.05 Mössbauer Analysis Software.[57] All isomer shifts refer to α-Fe at room temperature. Absence of any oxide impurities was checked by high velocity transmission measurements (v_{max} = 12 mm/s). Electrochemical data were recorded on a Metroohm Autolab potentiostat. The experiments were carried out in a three-electrode glass cell with a glassy carbon working electrode (d = 3mm), a platinum wire counter electrode, and a $Ag/AgNO_3$ (0.01 M in MeCN with 0.1 M Bu_4NBF_4) reference electrode. Voltammograms were recorded in MeCN with 0.1 M tetrabutylammonium tetrafluoroborate. All potentials are reported as versus the Fc/Fc^+ couple.

X-ray crystallography: All diffraction data were recorded on a MAR345 image plate using MoKα radiation generated by a Rigaku UltraX 18S rotating anode (Xenocs Fox3d mirrors). Prior to data collection the crystals were flash frozen to 150K. Data integration and reduction was performed by CrysAlisPR,[58] and the implemented absorption correction was applied. The structures were solved by SHELXT[59] and refined against F^2 by SHELXL-2014/7.[60] All non-hydrogen bonds were refined anisotropically, hydrogen atoms were added in calculated positions and refined in riding mode, with temperature factors 1.2 times higher than their parent atoms.

N,N,N',N'-tetrakis(3-pyridazylmethyl)-1,3-propylenediamine (L1) A solution of 3-(chloromethyl)pyridazine (1 eq., 1.75 g, 13.60 mmol) in CH_3CN (20 mL) was added to a solution of 1.,3-diaminopropane (0.17 eq., 194 µL, 2.33 mmol), K_2CO_3 (2 eq., 3.22g, 23.33 mmol) and KBr (1.5 eq., 2.08 g, 17.49 mmol) in CH_3CN (100 mL). The reaction mixture was heated at 40°C with an oil bath. The conversion of the reaction was monitored by ^{1}H NMR using dmso-*d*6 as solvent. Once the complete conversion of the 1,3-diaminopropane was observed (after ~ 7 days), the reaction was cooled to room temperature and filtered on a celite pad and the solid was washed twice with acetonitrile (2*100 mL). The solvent was evaporated under reduce pressure. The crude product was purified over basic alumina using 97% DCM/ 3% methanol as the eluent. The ligand was precipitated by slow addition of cyclohexane to its solution in DCM to give 0.55 g of **L1** (53%). ^{1}H NMR (300 MHz, $CDCl_3$) δ 9.07 (dd, *J* = 4.9, 1.8 Hz, 4H), 7.56 (dd, *J* = 8.4, 1.8 Hz, 4H), 7.45 (dd, *J* = 8.4, 4.9 Hz, 4H), 3.95 (s, 8H), 2.58 (t, *J* = 7.1 Hz, 4H), 1.81 (p, *J* = 7.4 Hz, 2H). ^{13}C NMR (75 MHz, $CDCl_3$) δ 161.22, 150.74, 127.08, 126.87, 58.03, 52.21, 24.86.

N,N'-bis(3-pyridazylmethyl)-N,N'-bis(2-pyridylmethyl)propylenediamine (**L2**) 3-(Chloro-methyl)pyradizine hydrochloride (3.1 g, 0.0189 mole) was added to a mixture of N,N-bis(2-pyridylmethyl)propylene diamine (2.5 g, 0.009 mole) and K_2CO_3 (7.4 g, 0.054 mole) in dry acetonitrile (150 mL) at room temperature. The mixture was heated to reflux and allowed to stir for 24 h under argon. The reaction was then cooled down to room temperature, and the solid was filtered off and the solvent removed by rotary evaporation. The crude product was purified over basic alumina using (97% DCM/ 3% methanol) to yield 2.64

g (66 %) of **L2**. ^{1}H NMR (300 MHz, Chloroform-*d*) δ 9.01 (dd, *J* = 4.9, 1.8 Hz, 2H), 8.48 (ddd, *J* = 4.9, 1.8, 0.9 Hz, 2H), 7.63 – 7.53 (m, 4H), 7.37 (dd, *J* = 8.4, 4.9 Hz, 2H), 7.30 (dt, *J* = 7.8, 1.1 Hz, 2H), 7.11 (ddd, *J* = 7.5, 4.9, 1.2 Hz, 2H), 3.91 (s, 4H), 3.73 (s, 4H), 2.59 – 2.47 (m, 4H), 1.85 – 1.70 (m, 2H). ^{13}C NMR (75 MHz, $CDCl_3$) δ 162.03, 159.19, 150.54, 149.22, 136.53, 126.73, 126.68, 123.07, 122.19, 60.41, 58.23, 52.42, 24.86.

(N,N,N',N'-tetrakis(2-pyridazylmethyl)propylenediamine)iron(II) hexafluorophosphate (**1**) To a solution of **L1** (0.10 g, 0.2 mmol) in distilled water (1.0 ml), was added $FeCl_2$ (0.029 g, 0.2 mmol) resulting in an immediate color change from yellow to dark red. The solution was allowed to stir at 80 ºC for 20 minutes after which time solid KPF_6 (0.083 g, 0.5 mmol) was added and the mixture was stirred for an additional 10 minutes at 80 ºC. The flask was then allowed to cool to room temperature, during which time a red solid precipitated from the solution. The solid was collected by filtration to give complex **1** (0.11 g, 62%) as a red microcrystalline solid. Single crystals suitable for X-ray analysis were obtained by the slow-diffusion method by first layering a solution of **1** in acetonitrile with hexane, followed by addition of toluene on top of the hexane layer. ^{1}H NMR (300 MHz, CD_3CN) δ 8.93 (d, J = 4.7 Hz, *2H*), 8.86 (d, J = 4.4, 2H Hz), 7.68 (d, J = 8.2 Hz, 2H), 7.61 (dd, J = 8.0, 4.7 Hz, 2H), 7.55 (dd, *J* = 8.5, 4.9 Hz, 2 H), 7.44 (d, J = 8.2 Hz, 2H), 4.89 (d, J = 19.7 Hz, 2H), 4.48 (d, J = 15.8 Hz, 2H), 4.30 (d, J = 19.7 Hz, 2H), 4.26 (d, J = 15.8 Hz, 2H), 3.32 (m, 2H), 2.58 – 2.35 (m, 4H) . ^{13}C NMR (75 MHz, CD_3CN) δ 170.55, 168.73, 165.76, 153.92, 151.93, 127.33, 126.91, 126.39, 125.54, 69.42, 63.46, 54.83, 22.22. HRMS for $C_{23}H_{26}N_{10}Fe^{2+}$ (-2PF_6) Theoretical: 248.08655; Experimental: 248.08635. UV-vis (MeCN) λ_{max} (nm) [ε (M^{-1},cm^{-1})] : 209 [15506], 242 [11795], 449 [13884]. Anal. Calc'd. for $C_{23}H_{26}F_{12}FeN_{10}P_2$ (788.29 g.mol-1): C, 35.04; H, 3.32; N, 17.76. Found: C, 34.6; H, 3.53; N, 17.37%.

(N,N'-bis(2-pyridazylmethyl)-N,N'-bis(2-pyridylmethyl)propylenediamine)iron(II) hexafluorophosphate (**2**) To a solution of **L2** (0.20 g, 0.5 mmol) in distilled water (3.0 ml), was added $FeCl_2$ (0.058 g, 0.5mmol) resulting in an immediate color change from yellow to dark red. The solution was allowed to stir at 80 ºC for 20 minutes after which time solid KPF_6 (0.167 g, 1.0 mmol) was added and the mixture was stirred for an additional 10 minutes at 80 ºC. The flask was then allowed to cool to room temperature, during which time a red solid precipitated from the solution. The solid was collected by filtration to give complex 2 (0.27 g, 76%) as a red microcrystalline solid. Single crystals suitable for X-ray analysis were obtained by the slow-diffusion method by first layering a solution of **2** in acetonitrile with hexane, followed by addition of toluene on top of the hexane layer. ^{1}H NMR (300 MHz, CD_3CN) δ 9.07 (d, 1H, J = 5.3 Hz), 8.97 (dd, *J* = 4.1, 2.3 Hz, 1H), 8.76 (dd, *J* = 5.3, 1.8 Hz, 1H), 7.86 (t, *J* = 7.6 Hz, 1H), 7.74 (t, J = 7.6 Hz, 1H), 7.64-7.56 (m, 4H), 7.46 (dd, J = 8.2, 4.7 Hz, 1H), 7.38-7.24 (m, 3H), 7.18 (t, J = 7.0 Hz, 1H), 4.86 (d, J = 20.5 Hz, 1H), 4.79 (d, J = 20.5 Hz, 1H), 4.39 (d, J = 15.8 Hz, 1H), 4.35 (d, J = 15.8 Hz, 1H), 4.20 (d, J = 18.2 Hz, 1H), 4.14 (d, J = 18.8 Hz, 1H), 4.10 (d, J = 15.8 Hz, 1H), 4.03 (d, J = 15.8 Hz, 1H), 3.30-3.15 (m, 2H), 2.62-2.52 (m, 1H), 2.37-2.34 (m, 3H); ^{13}C NMR (75 MHz, CD_3CN) δ 170.14, 166.72, 165.06, 161.77, 156.95, 154.34, 153.37, 152.82, 138.48, 138.18, 128.06, 126.89, 126.41, 125.37, 124.65, 123.62, 121.40, 70.52, 69.37, 65.04, 63.03, 54.42, 22.23. HRMS for $C_{25}H_{28}N_8Fe^{2+}$ (-2PF_6) Theoretical: 247.09135; Experimental: 247.09111. UV-vis (MeCN) λ_{max} (nm) [ε (M^{-1},cm^{-1})] 205 [14996], 249 [10793], 384 [5712], 458 [8601]. Anal. Calc'd. for $C_{25}H_{26}F_{12}FeN_8P_2$ (784.30 g.mol-1): C, 38.19; H, 3.59; N, 14.24. Found: C, 37.89; H, 3.87; N, 13.98%.

(N,N,N',N'-tetrakis(2-pyridylmethyl)propylenediamine)iron(II) hexafluorophosphate (**3**) To a solution of **L3** (0.50 g, 1.1 mmol) in distilled water (5.0 ml), was added $FeCl_2$ (0.144 g, 1.1mmol) resulting in an immediate color change from yellow to red. The solution was allowed to stir at 80 ºC for 20 minutes after which time solid KPF_6 (0.420 g, 2.3 mmol) was added and the mixture was stirred for an additional 10 minutes at 80 ºC. The flask was then allowed to cool to room temperature, during which time a red solid precipitated from the solution. The solid was collected by filtration to give complex **3** (0.73 g, 82%) as a red-orange microcrystalline solid. The metal complex was crystalized by layering acetonitrile onto a chloroform solution of **3**. ^{1}H NMR (300 MHz, CD_3CN) δ 8.66 (d, J = 5.3 Hz, 2H), 7.92 (d, J = 5.3 Hz, 4H), 7.88 (t, J = 7.6 Hz, 4H), 7.71-7.65 (m, 4H), 7.34 (t, J = 6.4 Hz, 2H), 7.25-7.20 (m, 4H), 4.79 (d, J = 20.3 Hz, 2H), 4.48 (d, J = 15.2 Hz, 2H), 4.12 (d, J = 15.8 Hz, 1*H*), 4.12 (d J = 19.3 Hz, 1H), 3.30 (m, 2H), 2.47-2.25 (m, 4H). ^{13}C NMR (300 MHz, CD_3CN) δ 166.07, 163.01, 157.00, 154.68, 138.34, 137.93, 125.96, 124.24, 121.39, 70.98, 64.41, 54.10, 22.29. HRMS for $C_{27}H_{30}N_6Fe^{2+}$ (-2PF_6) Theoretical: 246.09603; Experimental: 246.09586. UV-vis (MeCN) λ_{max} (nm) [ε (M^{-1},cm^{-1})] 205 [12865], 252 [10953], 386 (shoulder) [6350], 421 [7756]. Anal. Calc'd. for $C_{27}H_{30}F_{12}FeN_6P_2$ (784.34 g.mol-1): C, 41.35; H, 3.86; N, 10.71. Found: C, 41.36; H, 4.19; N, 10.45%.

Acknowledgements

This work was supported by the Université Catholique de Louvain Budget d'installation de Jeune Académique and Fonds Speciaux de Recherche FSR15 pour A. H. We also acknowledge support from the Fonds de la Recherche Scientifique-FNRS (PDR T.0102.15) and chargé de recherches fellowship to M. M. D. (16511866). We also thank the COST actions CM1305 and CA15128.

Keywords: iron, pyridazines, second coordination sphere, protonation, acid stability

CCDC 1824892-1824894 contain the supplementary crystallographic data for this paper. The data can be obtained free of charge from The Cambridge Crystallographic Data Centre via www.ccdc.cam.ac.uk/structures.

[1] L.-Y. Guo, S.-Y. Zeng, Z. Jaglicic, Q.-D. Hu, S.-X. Wang, Z. Wang, D. Sun, *Inorg. Chem* **2016**, *55*, 9006-9011.
[2] P. Jungk, F. Fischer, M. Hapke, *ACS Catal.* **2016**, *6*, 3025-3029.
[3] C. Di Giovanni, C. Gimbert-Surinach, M. Nippe, J. Benet-Buchholz, J. R. Long, X. Sala, A. Llobet, *Chem - Eur. J.* **2016**, *22*, 361-369.
[4] J. D. Vasta, K. A. Andersen, K. M. Deck, C. P. Nizzi, R. S. Eisenstein, R. T. Raines, *ACS Chem Biol.* **2016**, *11*, 193-199.

[5] S. Lense, A. Dutta, J. A. S. Roberts, W. J. Shaw, *Chem. Commun.* **2014**, *50*, 792-795.
[6] A. Dutta, S. Lense, J. A. S. Roberts, M. L. Helm, W. J. Shaw, *Eur. J. Inorg. Chem.* **2015**, *2015*, 5218-5225.
[7] L. Luo, H. Lin, L. Li, T. I. Smirnova, P. A. Maggard, *Inorg. Chem.* **2014**, *53*, 3464-3470.
[8] J. E. Clements, J. R. Price, S. M. Neville, C. J. Kepert, *Angew. Chem., Int. Ed.* **2016**, *55*, 15105-15109.
[9] S. Rodriguez-Jimenez, H. L. C. Feltham, S. Brooker, *Angew. Chem., Int. Ed.* **2016**, *55*, 15067-15071.
[10] W. A. Hoffert, M. T. Mock, A. M. Appel, J. Y. Yang, *Eur. J. Inorg. Chem.* **2013**, *2013*, 3846-3857.
[11] R. Benedix, H. Hennig, *Z. Anorg. Allg. Chem.* **1989**, *577*, 23-38.
[12] S. Brooker, R. J. Kelly, B. Moubaraki, K. S. Murray, *Chem. Commun.* **1996**, 2579-2580.
[13] S. Brooker, R. J. Kelly, P. G. Plieger, *Chem. Commun.* **1998**, 1079-1080.
[14] J. R. Price, Y. Lan, S. Brooker, *Dalton Trans.* **2007**, 1807-1820.
[15] J. R. Price, Y. Lan, B. Moubaraki, K. S. Murray, S. Brooker, *Aust. J. Chem.* **2010**, *63*, 779-784.
[16] Y. Li, X. Zhou, Z.-L. Chen, H.-H. Zou, F.-P. Liang, *Polyhedron* **2016**, *119*, 505-511.
[17] S. E. Bodman, C. M. Fitchett, *Dalton Trans.* **2014**, *43*, 12606-12613.
[18] K. V. Shuvaev, T. S. M. Abedin, C. A. McClary, L. N. Dawe, J. L. Collins, L. K. Thompson, *Dalton Trans.* **2009**, 2926-2939.
[19] K. V. Shuvaev, S. S. Tandon, L. N. Dawe, L. K. Thompson, *Chem. Commun.* **2010**, *46*, 4755-4757.
[20] N. K. Szymczak, L. A. Berben, J. C. Peters, *Chem. Commun.* **2009**, 6729-6731.
[21] R. Kositzki, S. Mebs, N. Schuth, N. Leidel, L. Schwartz, M. Karnahl, F. Wittkamp, D. Daunke, A. Grohmann, U.-P. Apfel, F. Gloaguen, S. Ott, M. Haumann, *Dalton Trans.* **2017**, *46*, 12544-12557.
[22] K. R. Gruenwald, M. Volpe, P. Cias, G. Gescheidt, N. C. Moesch-Zanetti, *Inorg. Chem.* **2011**, *50*, 7478-7488.
[23] G. Nuss, G. Saischek, B. N. Harum, M. Volpe, K. Gatterer, F. Belaj, N. C. Moesch-Zanetti, *Inorg. Chem.* **2011**, *50*, 1991-2001.
[24] M. Tuechler, S. Holler, J. A. Schachner, F. Belaj, N. C. Moesch-Zanetti, *Inorg. Chem.* **2017**, *56*, 8159-8165.
[25] M. Gryz, W. Starosta, J. Leciejewicz, *Acta Crystallogr., Sect. E: Struct. Rep. Online* **2006**, *62*, m3470-m3472.
[26] E. S. Ardiwinata, D. C. Craig, D. J. Phillips, *Inorg. Chim. Acta* **1989**, *166*, 233-238.
[27] C. R. Johnson, R. E. Shepherd, *Inorg. Chem.* **1983**, *22*, 3506-3513.
[28] C. R. Johnson, R. E. Shepherd, *Inorg. Chem.* **1983**, *22*, 2439-2444.
[29] M. N. Ackermann, L.-J. Kou, J. M. Richter, R. M. Willett, *Inorg. Chem.* **1977**, *16*, 1298-1301.
[30] J. R. Allan, G. A. Barnes, D. H. Brown, *J. Inorg. Nucl. Chem.* **1971**, *33*, 3765-3771.
[31] F. Roncaroli, R. Meier, *J. Coord. Chem.* **2015**, *68*, 2990-3002.
[32] J. K. McCusker, A. L. Rheingold, D. N. Hendrickson, *Inorg. Chem.* **1996**, *35*, 2100-2112.
[33] L. Lee, C.-H. Yuan, *J. Photochem. Photobiol., A* **1993**, *70*, 253-259.
[34] H. Toftlund, S. Yde-Andersen, *Acta Chem. Scand., Ser. A* **1981**, *A35*, 575-585.
[35] N. Segaud, J.-N. Rebilly, K. Senechal-David, R. Guillot, L. Billon, J.-P. Baltaze, J. Farjon, O. Reinaud, F. Banse, *Inorg. Chem.* **2013**, *52*, 691-700.
[36] N. Segaud, E. Anxolabehere-Mallart, K. Senechal-David, L. Acosta-Rueda, M. Robert, F. Banse, *Chem. Sci.* **2015**, *6*, 639-647.
[37] A. C. Bowman, C. Milsmann, E. Bill, Z. R. Turner, E. Lobkovsky, S. DeBeer, K. Wieghardt, P. J. Chirik, *J. Am. Chem. Soc.* **2011**, *133*, 17353-17369.
[38] D. N. Bowman, E. Jakubikova, *Inorg. Chem.* **2012**, *51*, 6011-6019.
[39] A. Thibon, J.-F. Bartoli, R. Guillot, J. Sainton, M. Martinho, D. Mansuy, F. Banse, *J. Mol. Catal. A: Chem.* **2008**, *287*, 115-120.
[40] A. Thibon, J.-F. Bartoli, S. Bourcier, F. Banse, *Dalton Trans.* **2009**, 9587-9594.
[41] M. Martinho, P. Dorlet, E. Riviere, A. Thibon, C. Ribal, F. Banse, J.-J. Girerd, *Chem. - Eur. J.* **2008**, *14*, 3182-3188.
[42] L. Duelund, R. Hazell, C. J. McKenzie, L. Preuss Nielsen, H. Toftlund, *J. Chem. Soc., Dalton Trans.* **2001**, 152-156.
[43] M. Tamura, Y. Urano, K. Kikuchi, T. Higuchi, M. Hirobe, T. Nagano, *Chem. Pharm. Bull.* **2000**, *48*, 1514-1518.
[44] J. K. McCusker, K. N. Walda, R. C. Dunn, J. D. Simon, D. Magde, D. N. Hendrickson, *J. Am. Chem. Soc.* **1992**, *114*, 6919-6920.
[45] J. K. McCusker, K. N. Walda, R. C. Dunn, J. D. Simon, D. Magde, D. N. Hendrickson, *J. Am. Chem. Soc.* **1993**, *115*, 298-307.
[46] J. K. McCusker, H. Toftlund, A. L. Rheingold, D. N. Hendrickson, *J. Am. Chem. Soc.* **1993**, *115*, 1797-1804.
[47] Y. Mori, M. Sato, T. Iida, *Chem. Lett.* **1992**, 469-472.
[48] P. DeBurgomaster, M. Bartholomae, R. Raffel, W. Ouellette, A. Mueller, J. Zubieta, *Inorg. Chim. Acta* **2010**, *363*, 1386-1394.
[49] M. G. N. Russell, R. W. Carling, J. R. Atack, F. A. Bromidge, S. M. Cook, P. Hunt, C. Isted, M. Lucas, R. M. McKernan, A. Mitchinson, K. W. Moore, R. Narquizian, A. J. Macaulay, D. Thomas, S.-A. Thompson, K. A. Wafford, J. L. Castro, *J. Med. Chem.* **2005**, *48*, 1367-1383.
[50] A. Bolaender, D. Kieser, C. Voss, S. Bauer, C. Schoen, S. Burgold, T. Bittner, J. Hoelzer, R. Heyny-von Haussen, G. Mall, V. Goetschy, C. Czech, H. Knust, R. Berger, J. Herms, I. Hilger, B. Schmidt, *J. Med. Chem.* **2012**, *55*, 9170-9180.
[51] B. Chen, X. Zhou, K. Taghizadeh, J. Chen, J. Stubbe, P. C. Dedon, *Chem. Res. Toxicol.* **2007**, *20*, 1701-1708.
[52] M. A. Ali, N. Bhogal, J. B. C. Findlay, C. W. G. Fishwick, *J. Med. Chem.* **2005**, *48*, 5655-5658.
[53] A. J. McCoy, R. W. Grosse-Kunstleve, P. D. Adams, M. D. Winn, L. C. Storoni, R. J. Read, *J. Appl. Crystallogr.* **2007**, *40*, 658-674.
[54] A. L. Spek, *Acta Crystallogr., Sect. C: Struct. Chem.* **2015**, *71*, 9-18.
[55] P. Mialane, A. Nivorojkine, G. Pratviel, L. Azema, M. Slany, F. Godde, A. Simaan, F. Banse, T. Kargar-Grisel, G. Bouchoux, J. Sainton, O. Horner, J. Guilhem, L. Tchertanova, B. Meunier, J.-J. Girerd, *Inorg. Chem.* **1999**, *38*, 1085-1092.
[56] M. Tretbar, C. B. W. Stark, *Eur. J. Org. Chem.* **2017**, *2017*, 6942-6946.
[57] K. R. Lagrec, D. G. in *Recoil, Mossbauer Spectral Analysis Software for Windows [1.0];*, *Vol.* Department of Physics, University of Ottawa: Canada, **1998**.
[58] *CrysAlisPRO Software System*, *Vol.* Rigaku Corporation: Oxford, UK, **2015**.
[59] G. M. Sheldrick, *Acta Crystallogr., Sect. C: Struct. Chem.* **2015**, *71*, 3-8.
[60] G. M. Sheldrick, *Acta Crystallogr., Sect. A: Found. Adv.* **2015**, *71*, 3-8.

10.1002/ejic.201800533

WILEY-VCH

Entry for the Table of Contents

FULL PAPER

The synthesis and characterization of a series of pyridazine/pyridine containing octahedral iron(II) complexes and their reactivity towards protonation is described. The presence of additional basic sites in the second coordination sphere greatly enhances the acidic stability of the complexes but only when the pyridazine groups are positioned in a way that allows them to act in a cooperative manner.

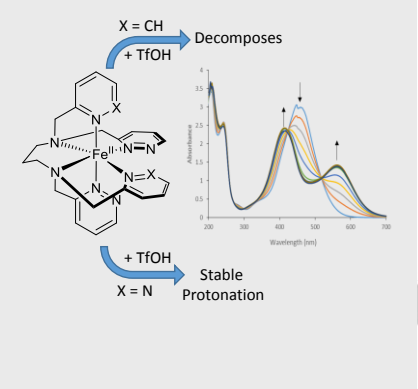

Stabilizing Protonated Complexes

Ahmad Hammoud, Jean-Boris Nshimyumuremyi, Jérémie Bourotte, Fabio Lucaccioni, Koen Robeyns, Marinela M. Dîrtu, Yann Garcia, Michael L. Singleton**

Page No. – Page No.
Cooperative interactions in the second coordination sphere of pyridazine/pyridine containing polyazaheterocyclic iron(II) complexes increase their stability towards protonation.